IEEE Access
Multidisciplinary ⋮ Rapid Review ⋮ Open Access Journal

Received July 24, 2019, accepted August 10, 2019, date of publication September 11, 2019, date of current version September 26, 2019.

Digital Object Identifier 10.1109/ACCESS.2019.2940434

Dynamic Handling Characteristics Control of an in-Wheel-Motor Driven Electric Vehicle Based on Multiple Sliding Mode Control Approach

MINSEONG CHAE[1,*], YOUNGJIN HYUN[2,*], KYONGSU YI[2], AND KANGHYUN NAM[1], (Member, IEEE)
[1]Department of Mechanical Engineering, Yeungnam University, Gyeongsan 712-749, South Korea
[2]Department of Mechanical Engineering, Seoul National University, Seoul 08826, South Korea

Corresponding author: Kanghyun Nam (khnam@yu.ac.kr)

This work was supported by the Basic Science Research Program through the National Research Foundation of Korea (NRF) Funded by the Ministry of Education (2017R1A4A1015581) and by the National Research Foundation of Korea (NRF) Grant Funded by Yeungnam University Research Grant 217A580015.

*Minseong Chae and Youngjin Hyun are co-first authors.

ABSTRACT This paper presents an advanced motion control method based on the multiple adaptive sliding mode control (MASMC) approach used in torque vectoring technology to improve the handling performance of fully electric vehicles. During cornering, a driver can reduce their handling manipulation effort via torque vectoring, implying that the vehicle has a large side-slip angle. In control design, MASMC has a cascade structure for the safety system. Additionally, for robust control, adaptive sliding mode control is used to address the problem of varying parameters. The stability of the entire control system is proved by Lyapunov stability theory. Moreover, optimal torque distribution, which is based on the minimization of actuator redundancy, is proposed in this paper to avoid the excessive saturation of the actuator. The effectiveness of the proposed MASMC is tested using CarSim and a MATLAB/Simulink environment. It is confirmed that the handling manipulation effort is reduced by more than 60% in comparison to that without any control, and it is also reduced by approximately 40% compared to a conventional control method. Moreover, because of the parameter adaptation effect, the unnecessary chattering of in-wheel-motor torque is decreased.

INDEX TERMS Electric vehicles, torque vectoring, adaptive sliding mode control, sideslip angle, advanced motion control.

I. INTRODUCTION

Unlike internal combustion engine vehicles, in-wheel-motor electric vehicles with active steering have significant benefits in terms of energy efficiency and motion control. These benefits are as follows [1]: i) the torque response of driving motors is very fast and accurate; ii) all wheels can be controlled independently; iii) the driving torque can be easily measured from the motor current; and iv) the braking force can be regenerated. Based on these benefits, over the past few years, a great deal of research on the advanced dynamics control of electric vehicles has been conducted [2]–[6]. The purpose of advanced motion control research is to maintain the stability and controllability of a vehicle by eliminating unintended vehicle behavior with active vehicle control. The main control objective of the motion control system is to control factors such as anti-slip, zero- yaw rate, zero-side-slip, and prevention of rollover by implementing an integrated chassis control system including differential braking, active steering, and suspension. For vehicle safety control, Beal and Gerdes [7] used model predictive control for actuating an active steering system to limit the vehicle side-slip angle in emergency situations.

Recently, developing high performance electric vehicles has become a priority for research and development. For example, [8], [9] are quality studies of high-performance electric vehicles. In particular, the Fun to Drive model is noteworthy in the field of high performance electric vehicles as it offers the pleasure of "real driving", in that the car and driver can communicate with acceleration and cornering freely. Slippage between the tire and road is commonly observed in motor sports, and skilled drivers use this phenomenon called "drifting" as a technique to escape corners at a high speed [10]. Skilled drivers drift by reducing the rear tire

The associate editor coordinating the review of this manuscript and approving it for publication was Nasim Ullah.

lateral force, and they drift the vehicle to control the vehicle heading angle. One type of solution to realize Fun to Drive for the common driver is by providing safe drifting capacity, as used by skilled drivers. Drifting is related to large side-slip angles (i.e. when the saturation of driving force occurs), and this makes controller design more difficult than safe driving, which is characterized by small side-slip angles and linear friction tire properties [11], [12].

Vehicle motion control with large side-slip angles has already been investigated. In [13], the stability analysis of vehicle motion using phase portrait analysis for a case that includes a large side-slip angle was examined. In [14], [15], they investigated how a skilled driver operates the vehicle outside the stable regions of vehicle dynamics to achieve agility performance. In [16], stability analysis of equilibrium points of drifting was used to demonstrate that drifting is a motion around unstable equilibrium points for a rear-wheel drive vehicle. To control large side-slip angles, torque vectoring, which is also called yaw moment control, is primarily used by the distribution of the wheel torque individually. The advantages of torque vectoring can be summarized as follows [17]:

1) Shaping the understeer characteristic in quasi-static conditions
2) Enhancing the transient cornering response
3) Improving handling performance

In [17], the integrated control method of yaw rate and side-slip angle control was presented for realizing the effective torque vectoring. However, the integrated and continuous control systems may be lost stability in unfavorable driving conditions due to different dynamic characteristics between yaw rate and side-slip angle.

In this paper, we focus on improving handling performance by the torque vectoring method based on the MASMC approach, which is composed of a yaw rate controller and side-slip angle controller. Torque vectoring control must not affect the vehicle safety system when drivers confront emergency situations. Consequently, there are two types of driving modes, the safety mode and dynamic mode. Furthermore, the optimal torque distribution law, which creates the reference of individual in-wheel-motor torque and front lateral force, is used in the entire algorithm to prevent excessive saturation of driving force. The optimal torque distribution is based on the minimization of actuator redundancy. For reducing actuator redundancy, the concept of the workload function, which is the ratio of the current tire force to the maximum generated tire force, is used in the optimal torque distribution. To generate front lateral force, an active front steering system is used [18]. To evaluate the performance of the proposed MASMC approach, simulation results are compared with the results based on the conventional method (i.e. yaw rate control). The remainder of this paper is organized as follows: Section II presents vehicle modeling, tire modeling, and dynamic system modeling; Section III presents the proposed MASMC method; Section IV presents the optimal torque distribution based on least squares method; Section V presents simulation results compared with the conventional method; finally, Section VI presents conclusions and future research directions.

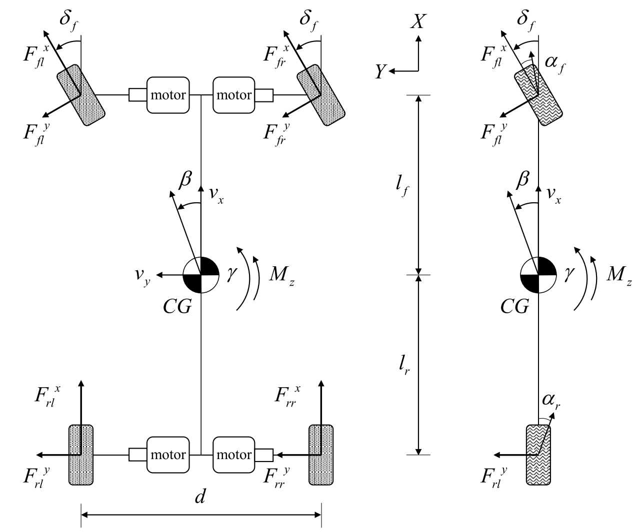

FIGURE 1. Vehicle yaw plane model. (a) Three-DOF model. (b) Two-DOF model (i.e., bicycle model).

II. VEHICLE SYSTEM MODELING

A. VEHICLE MODELING

In this section, a three degree-of-freedom (3-DOF) yaw plane model is introduced to describe the lateral motion of an electric vehicle having four-in-wheel-motors that can be driven independently and has active front steering systems. A simplified two-degree-of-freedom (2-DOF) yaw plane model, namely a single-track model or bicycle model, is used for the control design. The two types of yaw plane model representations are shown in Fig. 1.

The governing equations for lateral and yaw motions are given by

$$mv_x(\dot{\beta}+\gamma) = F_f^y\cos\delta_f + F_r^y \approx F_f^y + F_r^y \tag{1}$$

$$I_z\dot{\gamma} = l_f F_f^y \cos\delta_f - l_r F_r^y + M_z \approx l_f F_f^y - l_r F_r^y + M_z \tag{2}$$

where front lateral tire force F_f^y is the sum of the front left and right lateral tire forces(i.e., $F_f^y = F_{fl}^y + F_{fr}^y$). The yaw moment M_z is a direct yaw moment input, which is induced by the independent torque control of in-wheel-motors, and can be calculated as follows:

$$\begin{aligned} M_z = l_f F_f^y\cos\delta_f - l_r F_r^y + F_{fl}^x\left(l_f\sin\delta_f - \frac{d}{2}\cos\delta_f\right) \\ + F_{fr}^x\left(l_f\sin\delta_f + \frac{d}{2}\cos\delta_f\right) - \frac{d}{2}F_{rl}^x + \frac{d}{2}F_{rr}^x \end{aligned} \tag{3}$$

Equations (1)–(2) are simplified with small angle approximation (i.e., $\delta_f \ll 1$)

B. LINEAR TIRE MODELING

To model the tire force, several tire models have been used. In this study, we use linearized tire models to avoid complex calculations. For small tire slip angles, the linearized lateral tire forces are defined as follows:

$$F_f^y = -2C_f\alpha_f = -2C_f\left(\beta + \frac{\gamma l_f}{v_x} - \delta_f\right) \quad (4)$$

$$F_r^y = -2C_r\alpha_r = -2C_r\left(\beta - \frac{\gamma l_r}{v_x}\right) \quad (5)$$

C. DYNAMIC SYSTEM MODELING

From (1),(2),(4) and (5), the dynamic equations for side-slip angle and yaw rate can be derived as follows:

$$\begin{aligned}\dot{\beta} &= -\frac{2(C_f + C_r)}{mv_x}\beta + \left(\frac{2(l_rC_r - l_fC_f)}{mv_x^2} - 1\right)\gamma \\ &\quad + \frac{2C_f}{mv_x}\delta_f \end{aligned} \quad (6)$$

$$\begin{aligned} I_z\dot{\gamma} &= -\frac{2(l_f^2C_f + l_r^2C_r)}{v_x}\gamma + 2(l_rC_r - l_fC_f)\beta \\ &\quad + 2l_fC_f\delta_f + M_z \end{aligned} \quad (7)$$

In this study, we can control yaw rate by the yaw moment Mz in the yaw rate dynamic. Then, we can also control the side-slip angle by yaw rate in the side-slip angle dynamic. To summarize, we have designed the cascade structure for side-slip angle control; thereby, we can design the divided controllers according to the safety driving mode and dynamic driving mode. The safety mode is a basic mode of a motion control system that forces the vehicle to maintain a stable yaw rate by intercepting the side-slip angle controller. In contrast, dynamic mode, which is based on side-slip angle control, is a selective option where both system and driver make decisions for which they require dynamic mode for improved handling.

We can rearrange equations in state space form from (6)–(7) as follows [19]:

$$\begin{aligned}\dot{x}(t) &= Ax(t) + Bu(t) \\ y(t) &= Cx(t)\end{aligned} \quad (8)$$

where $x = [\beta, \gamma]^\mathsf{T}$, $u = \left[\delta_f, M_z\right]^\mathsf{T}$, $y = \beta$, and

$$A = \begin{bmatrix} \frac{-2(C_f + C_r)}{mv_x} & \frac{2(l_rC_r - l_fC_f)}{mv_x^2} - 1 \\ \frac{2(l_rC_r - l_fC_f)}{I_z} & \frac{-2(l_f^2C_f - l_r^2C_r)}{I_zv_x}\end{bmatrix}$$

$$B = \begin{bmatrix} \frac{2\,C_f}{mv_x} & 0 \\ \frac{2\,l_fC_F}{I_z} & \frac{1}{I_z}\end{bmatrix}, \quad C = \begin{bmatrix}1 & 0\end{bmatrix} \quad (9)$$

Then, there are two states to be controlled and two controllable inputs. Moreover, we can see that the variance of vehicle velocity v_x and cornering stiffness $C_{f,r}$ make considerable changes in the vehicle dynamics(i.e., a natural frequency and damping coefficient of the vehicle dynamics). Therefore, we have to design a robust controller to prevent this undesirable effect.

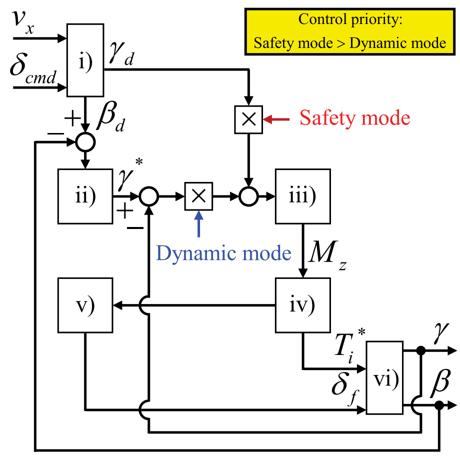

FIGURE 2. Overall control scheme of proposed MASMC. (i) Desired vehicle model. (ii) Outer beta controller. (iii) Inner yaw controller. (iv) Optimal torque distribution. (v) Active front steering. (vi) CarSim vehicle model.

III. MOTION CONTROL BASED ON MASMC

The entire scheme of the proposed MASMC is shown in Fig. 2. The system includes the following parts: generators that create the desired vehicle lateral acceleration, yaw rate and side-slip angle, an outer adaptive sliding mode control algorithm for generating the reference yaw-rate, an inner adaptive sliding mode control algorithm for generating the yaw moment, a torque distribution law for minimizing actuator redundancy and a CarSim vehicle model to verify the performance of the proposed MASMC.

A. DESIRED VEHICLE MODEL

In this study, the objective of vehicle motion control is to improve the vehicle handling performance and maintain stability under various driving conditions. In particular, for cornering maneuvers, side-slip angle β of the vehicle should be close to the desired vehicle responses and the desired yaw rate γ is required for safety. The desired vehicle responses are based on the driver's cornering intention(i.e., driver's steering command and vehicle speed). Commonly, $\dot{\beta} = \dot{\gamma} = 0$ during steady-state cornering.

The desired vehicle lateral acceleration, yaw rate and side-slip angle are defined as follows:

$$a_{y,d} = v_x(\gamma_d + \dot{\beta}_d) \quad (10)$$

$$\gamma_d = \frac{1}{1+\tau_\gamma}\cdot\frac{1}{1+K_sv_x^2}\cdot\frac{v_x}{l}\cdot\delta_{cmd} \quad (11)$$

$$\beta_d = \frac{1}{1+\tau_\beta}\cdot\frac{1-(\frac{ml_fv_x^2}{2ll_rC_r})}{1+K_sv_x^2}\cdot\frac{v_x}{l}\cdot\delta_{cmd} \quad (12)$$

$$K_s = \frac{m(l_rC_r - l_fC_f)}{2l^2C_fC_r} \quad (13)$$

where τ_γ and τ_β are the relaxation time constants of the desired model filters, and K_s is the vehicle stability factor, which describes the steering characterisristics of the vehicle.

The sign of $(l_r C_r - l_f C_f)$ represents the vehicle motion behavior by steering.

The steering characteristics are classified as follows:

$$\begin{cases} l_r C_r - l_f C_f > 0, & \text{under steering} \\ l_r C_r - l_f C_f = 0, & \text{neutral steering} \\ l_r C_r - l_f C_f < 0, & \text{over steering} \end{cases} \tag{14}$$

B. DESIGN OF THE INNER ASMC

The main objective of the motion control system, which has some critical issues, is to track the desirable side-slip angle when drivers decide to turn the corner or rapidly change lanes for dynamic driving. The critical issues are that vehicles have a great deal of varying parameters when dynamically driving (e.g., cornering stiffness $C_{f,r}$, friction coefficient $\mu, \ldots$) and the assumptions of vehicle model dynamics for avoiding complex calculations cause high nonlinearity. These issues contribute to the high nonlinearity of whole vehicle motion for various driving maneuvers. To solve nonlinear system control, the sliding mode control (SMC) approach is an effective strategy because of the robustness against disturbances or model uncertainties. Moreover, the SMC has other advantages, such as stabilizing high nonlinear systems that are difficult to control by controlling the continuous-state feedback laws, fast response time, and good transient performance [20]–[23].

Typically, in the sliding mode control design, the control makes the system to slide on a certain surface which guarantees the achievement of the control objective. To achieve the inner control objective which is tracking the reference yaw rate made by outter SMC (i.e., $\lim_{t\to\infty} S_1(t) = 0$), the sliding surface $S_1(t)$ is defined as

$$S_1 = \gamma - \gamma_d \tag{15}$$

Then, we can see that the sliding surface $S_1(t) = 0$ denotes no tracking error of yaw rate. The time derivative of (15), yields

$$\dot{S}_1 = \dot{\gamma} - \dot{\gamma}_d \tag{16}$$

Using (7) and (16) yields

$$\dot{S}_1 = -\frac{2(l_f^2 C_f + l_r^2 C_r)}{I_z v_x}\gamma + \frac{2(l_r C_r - l_f C_f)}{I_z}\beta + \frac{2 l_f C_f}{I_z}\delta_f + \frac{M_z}{I_z} + \frac{M_d}{I_z} - \dot{\gamma}_d \tag{17}$$

where M_d is newly defined as a yaw moment of the disturbance mainly caused by lateral wind and unbalanced road conditions. To achieve the control requirement, a reaching surface to be satisfied is designed as follows:

$$\dot{S}_1 = -k_{p1} S_1 - k_{s1} \cdot sgn(S_1) \tag{18}$$

where k_{p1} and k_{s1} are the positive control parameters selected to decide reaching speed and convergence rate of a tracking error. Additionally, k_{s1} should be tuned according to boundaries of uncertainties and disturbances. The inner sliding mode control law M_z derived from (17) and (18) is

$$M_z = I_z\dot{\gamma}_d + \frac{2B}{v_x}\gamma + 2A\beta - 2l_f C_f \delta_f - I_z k_{p1} S_1 - I_z k_{s1} \cdot sgn(S_1) \tag{19}$$

where A is defined as a yaw spring coefficient (i.e., $A = l_r C_r - l_f C_f$) and B is defined as a yaw damping coefficient (i.e., $B = l_f^2 C_f + l_r^2 C_r$), which vary with cornering stiffness.

There are two types of model uncertainties, unmodeled nonlinear dynamic uncertainties such as assumptions for calculation simplification and parametric uncertainties such as varying parameters. In designing an SMC, only a robust term like signum or saturation function overcomes these two model uncertainties to obtain robust stability. The model uncertainties, especially the parametric uncertainties, increase the gain of these robust terms to obtain the same tracking performance. As a result, the higher gain creates unnecessary chattering, causing uncomfortable feelings to drivers. To reduce the high gain chattering due to varying parameters, we applied adaptive control strategy. Thus, the control law M_z is modified as

$$M_z = I_z\dot{\gamma}_d + \frac{2\hat{B}}{v_x}\gamma + 2\hat{A}\beta - 2l_f \hat{C}_f \delta_f - k_{p1} S_1 - k_{s1} \cdot sgn(S_1) \tag{20}$$

where the adaptation laws for the updated parameters $\hat{A}$, $\hat{B}$ and $\hat{C}_f$ are chosen as

$$\begin{aligned} \dot{\hat{A}}(t) &= -\frac{2k_1}{I_z}\beta(t)S_1 - \eta_1 k_1 \tilde{A} \\ \dot{\hat{B}}(t) &= -\frac{2k_2}{I_z v_x}\gamma(t)S_1 - \eta_2 k_2 \tilde{B} \\ \dot{\hat{C}}_f(t) &= -\frac{2k_3 l_f}{I_z}\delta_f(t)S_1 - \eta_3 k_3 \tilde{C}_f \end{aligned} \tag{21}$$

Here, $\tilde{A} = \hat{A}(t) - A$, $\tilde{B} = \hat{B}(t) - B$, $\tilde{C}_f = \hat{C}_f(t) - C$, $k_i (i = 1, 2, 3)$ is the positive constant adaptation gain which determines the update rate and $\eta_i (i = 1, 2, 3)$ is the positive constant.

To prove the stability of the inner designed control system, the following positive definite Lyapunov function is considered.

$$V_1 = \frac{1}{2}S_1^2 + \frac{1}{2k_1}\tilde{A}^2 + \frac{1}{2k_2}\tilde{B}^2 + \frac{1}{2k_3}\tilde{C}_f^2 \tag{22}$$

Taking the time derivative of (22), substituting for $\dot{s}_1$ from (17), and plugging in the control law M_z and adaptation laws, we get:

$$\begin{aligned} \dot{V}_1 &= S_1\dot{S}_1 + \frac{1}{k_1}\tilde{A}\dot{\hat{A}} + \frac{1}{k_2}\tilde{B}\dot{\hat{B}} + \frac{1}{k_3}\tilde{C}_f\dot{\hat{C}}_f \\ &= S_1\left[-\frac{2B}{I_z v_x}\gamma + \frac{2A}{I_z}\beta + \frac{2l_f C_f}{I_z}\delta_f + \frac{M_z}{I_z} + \frac{M_d}{I_z} - \dot{\gamma}_d\right] \\ &\quad + \frac{1}{k_1}\tilde{A}\dot{\hat{A}} + \frac{1}{k_2}\tilde{B}\dot{\hat{B}} + \frac{1}{k_3}\tilde{C}_f\dot{\hat{C}}_f \\ &= S_1\left[\frac{2\gamma}{I_z v_x}\tilde{B} - \frac{2\beta}{I_z}\tilde{A} - \frac{2l_f\delta_f}{I_z}\tilde{C}_f - k_{p1}S_1 - k_{s1}\cdot sgn(S_1) + \frac{M_d}{I_z}\right] \end{aligned}$$

$$
\begin{aligned}
&+\frac{1}{k_1}\tilde{A}\left(-\frac{2k_1}{I_z}\beta(t)S_1-\eta_1 k_1\tilde{A}\right)\\
&+\frac{1}{k_2}\tilde{B}\left(-\frac{2k_2}{I_z v_x}\gamma(t)S_1-\eta_2 k_2\tilde{B}\right)\\
&+\frac{1}{k_3}\tilde{C}_f\left(-\frac{2k_3 l_f}{I_z}\delta_f(t)S_1-\eta_3 k_3\tilde{C}_f\right)\\
&\le -k_{p1}S_1^2-k_{s1}\left|S_1\right|+\left|S_1\right|\cdot\left|\frac{M_d}{I_z}\right|-\eta_1\tilde{A}^2-\eta_2\tilde{B}^2-\eta_3\tilde{C}_f^2
\end{aligned}
\tag{23}
$$

Define $\Gamma = sup_{t\ge 0}\left|\frac{M_d}{I_z}\right|$. If $k_{s1} > \Gamma$, we can rewritten (21) as

$$
\begin{aligned}
\dot{V}_1 &\le -k_{p1}S_1^2-k_{s1}\left|S_1\right|+\left|S_1\right|\cdot\left|\frac{M_d}{I_z}\right|-\eta_1\tilde{A}^2-\eta_2\tilde{B}^2-\eta_3\tilde{C}_f^2\\
&= -k_{p1}S_1^2-\left|S_1\right|\cdot\left(k_{s1}-\left|\frac{M_d}{I_z}\right|\right)-\eta_1\tilde{A}^2-\eta_2\tilde{B}^2-\eta_3\tilde{C}_f^2\\
&\le -k_{p1}S_1^2-\left|S_1\right|\cdot(k_{s1}-\Gamma)-\eta_1\tilde{A}^2-\eta_2\tilde{B}^2-\eta_3\tilde{C}_f^2<0
\end{aligned}
\tag{24}
$$

The function $V_1(t)$ is a positive definite and $\dot{V}_1(t)$ is a negative semi-definite. Moreover, $V_1(t)$ tends to infinity as $S_1(t)$ tends to infinity, therefore, because of Lyapunov's direct method, the equilibrium at the orgin $S_1(t) = 0$ is globally stable and the variable $S_1(t)$ is bounded. To compound the above conclusions, we can prove that the stability of the proposed control law, which is the satisfied control objective, i.e., $S_1(t) \to 0$ as $t \to \infty$, according to Lyapunov stability theory.

C. DESIGN OF THE OUTER ASMC

As in the inner ASMC design, the control makes the system slide on a certain surface which guarantees the achievement of the control objective. To achieve the outer control objective which is tracking the desired side-slip angle, i.e., $\lim_{t\to\infty} S_2(t) = 0$, the sliding surface $S_2(t)$ is defined as:

$$S_2 = \beta - \beta_d \tag{25}$$

Then, we can see that the sliding surface $S_2(t) = 0$ means a zero-tracking error of side-slip angle. From the time derivative of (25), we get

$$\dot{S}_2 = \dot{\beta} - \dot{\beta}_d \tag{26}$$

Using (6) and (26) yields

$$\dot{S}_2=-\frac{2(C_f+C_r)}{mv_x}\beta+\left(\frac{2(l_rC_r-l_fC_f)}{mv_x^2}-1\right)\gamma+\frac{2C_f}{mv_x}\delta_f-\dot{\beta}_d \tag{27}$$

To achieve the control requirement, a reaching surface to be satisfied is designed as follows:

$$\dot{S}_2 = -k_{p2}S_2 - k_{s2}\cdot sgn(S_2) \tag{28}$$

where k_{p2} and k_{s2} are the parameters that follow the same rule of the inner yaw rate SMC. The outer sliding mode control law γ, derived from (27) and (28) is:

$$\gamma = D\left[\dot{\beta}_d+\frac{2(C_f+C_r)}{mv_x}\beta-\frac{2C_f}{mv_x}\delta_f-k_{p2}S_2-k_{s2}\cdot sgn(S_2)\right] \tag{29}$$

We can apply the adaptation effect in (29) without a complex design process by deriving from the equality relationship between a yaw spring coefficient A and front cornering stiffness C_f in (19). Then, the outer sliding mode control law (29) can be rewritten as

$$\gamma=\hat{D}\left[\dot{\beta}_d+\frac{2(\hat{C}_f+\hat{C}_r)}{mv_x}\beta-\frac{2\hat{C}_f}{mv_x}\delta_f-k_{p2}S_2-k_{s2}\cdot sgn(S_2)\right] \tag{30}$$

where $\hat{C}_r$ is the estimated rear cornering stiffness and $\hat{D}$ is newly defined for the avoiding complex equation (i.e., $\hat{D}=\frac{mv_x^2}{2\hat{A}-mv_x^2}$).

We proved the stability of the outer designed control system as we analyzed the inner ASMC. The positive definite V_2 is defined as

$$V_2 = \frac{1}{2}S_2^2 \tag{31}$$

Taking the time derivative of (31), substituting for $\dot{s}_2$ from (27), and plugging in the modified control law γ, we obtain

$$
\begin{aligned}
\dot{V}_2 &= S_2\dot{S}_2\\
&= S_2\left[-\frac{2(C_f+C_r)}{mv_x}\beta+\left(\frac{2(l_rC_r-l_fC_f)}{mv_x^2}-1\right)\gamma\right.\\
&\quad\left.+\frac{2C_f}{mv_x}\delta_f-\dot{\beta}_d\right]\\
&= S_2\left[-k_{p2}S_2-k_{s2}\cdot sgn(S_2)\right]\\
&= -k_{p2}S_2^2-k_{s2}\left|S_2\right|<0
\end{aligned}
\tag{32}
$$

We can see that the outer sliding mode control law makes the closed loop control system asymptotically stable by Lyapunov stability theory. It is clear that entire proposed control system is asymptotically stable owing to the cascade structure of the controller.

The control laws of the proposed MASMC (i.e., equations (20) and (30)) have the discontinuity term, $sgn(S)$, which may lead to the undesirable chattering problem. A solution is proposed by replacing a discontinuous switching function with a saturation function, having the boundary layer thickness Φ as the continuous approximation of a signum function as follows:

$$
\begin{aligned}
sgn(S_i) &\approx sat\left(\frac{S_i}{\Phi_i}\right)\\
&=\begin{cases}\dfrac{S_i}{\Phi_i}, & \text{if } \left|\dfrac{S_i}{\Phi_i}\right|<1\\[2ex] sgn\left(\dfrac{S_i}{\Phi_i}\right), & \text{otherwise} \quad (i=1,2).\end{cases}
\end{aligned}
\tag{33}
$$

where Φ_i are the low values selected arbitrarily such that the chattering phenomenon can be decreased.

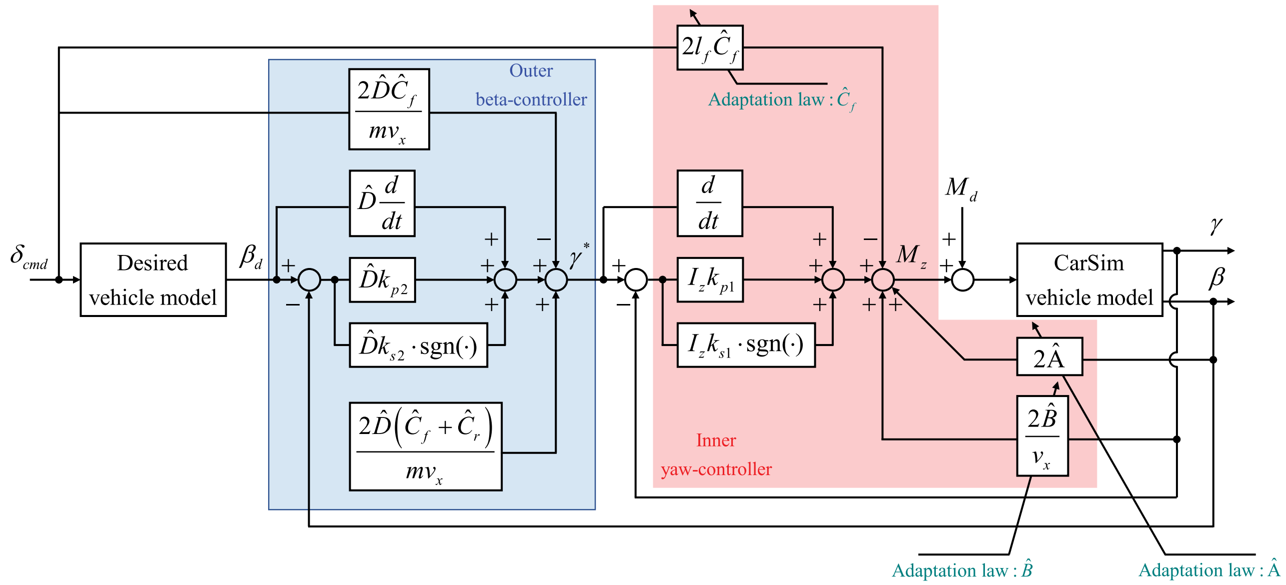

FIGURE 3. Synthesis control scheme of MASMC.

Finally, two types of modes can be used in the proposed MASMC owing to the cascade structure, the safety mode and dynamic mode. The synthesis control scheme is shown in Fig. 3.

IV. OPTIMAL TORQUE DISTRIBUTION (OTD)

A. PROBLEM STATEMENT

As previously introduced, an optimal torque distribution method that uses an active front steering system with four in-wheel-motors is described in this section. Because our system to be controlled has three control inputs and five controllable outputs, we should consider the actuator redundancy issue to avoid the saturation of driving and lateral forces [24]–[26]. The five control variables need satisfy the following equality constraints given by force and moment balance equations.

1) LONGITUDINAL BALANCE

The sum of the generated longitudinal tire forces on the four wheels must be equal to the required total longitudinal force to satisfy the driver's pedal command.

$$F_{cmd} = F_f^y \sin\delta_f + F_{fl}^x \cos\delta_f + F_{fr}^x \cos\delta_f + F_{rl}^x + F_{rr}^x \tag{34}$$

2) LATERAL BALANCE

The sum of the generated lateral tire forces on the four wheels must be equal to the required total lateral force to follow the desired lateral force.

$$ma_{y,d} = F_f^y \cos\delta_f + F_r^y + F_{fl}^x \sin\delta_f + F_{fr}^x \sin\delta_f \tag{35}$$

3) MOMENT BALANCE

The sum of the generated moment by longitudinal and lateral tire forces must be equal to the required total yaw moment to meet desired yaw rate response.

$$\begin{aligned} M_z = {} & l_f F_f^y \cos\delta_f - l_r F_r^y + F_{fl}^x \left(l_f \sin\delta_f - \frac{d}{2}\cos\delta_f \right) \\ & + F_{fr}^x \left(l_f \sin\delta_f + \frac{d}{2}\cos\delta_f \right) - \frac{d}{2} F_{rl}^x + \frac{d}{2} F_{rr}^x \end{aligned} \tag{36}$$

Moreover, the relation between three tire forces(longitudinal tire force F_i^x, lateral tire force F_i^y and vertical tire force F_i^z) should satisfy the following equation:

$$\sqrt{F_i^{x2} + F_i^{y2}} \le \mu_{max} F_i^z \tag{37}$$

From (37), we can confirm that it is a circle which implies that the resultant force of F_i^x and F_i^y cannot exceed the maximum tire force $\mu_{max} F_i^z$. This circle is called the friction circle. The vertical tire force F_i^z is obtained from the following equations in which the effects of weight transfer according to longitudinal and lateral accelerations are described:

$$\begin{aligned} F_i^z &= mg \left[\frac{l_r}{2l} - \frac{a_x}{g}\frac{h_{CG}}{2l} \mp \frac{a_y}{g}\frac{l_r h_{CG}}{dl} \right], \quad i = fl, fr \\ F_i^z &= mg \left[\frac{l_r}{2l} + \frac{a_x}{g}\frac{h_{CG}}{2l} \mp \frac{a_y}{g}\frac{l_r h_{CG}}{dl} \right], \quad i = rl, rr \end{aligned} \tag{38}$$

As aforementioned, the tire workload, which is the rate of the maximum tire force that can be generated in a friction circle against the current resultant force is a critical indicator of tire force saturation. The workloads function η_i is defined as follows:

$$\eta_i = \frac{\sqrt{F_i^{x2} + F_i^{y2}}}{\mu_{max} F_i^z} \tag{39}$$

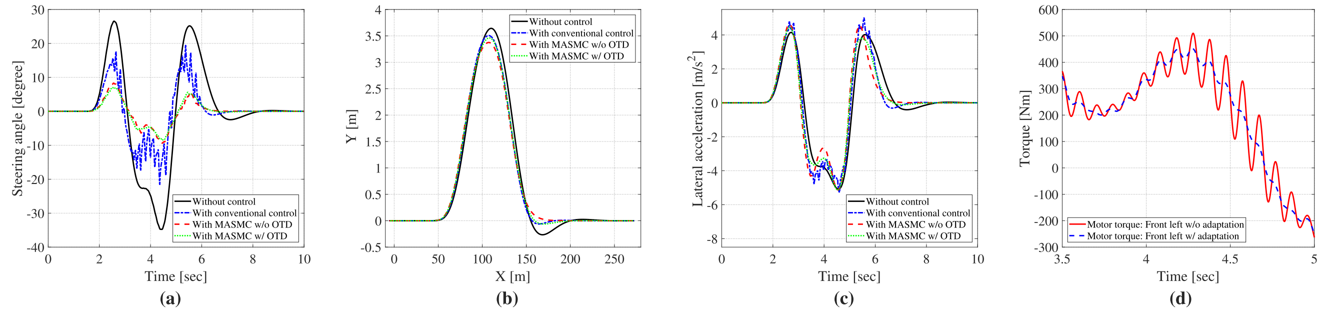

FIGURE 4. Comparsion of the three methods. (a) Steering wheel angle. (b) Trajectory. (c) Lateral acceleration. (d) Adaptation effect.

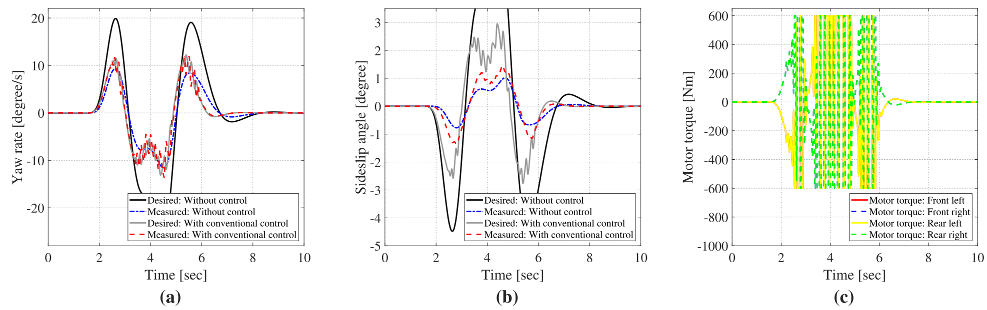

FIGURE 5. Driving data of conventional control. (a) Yaw rate. (b) Side-slip angle. (c) In-wheel-motor torque.

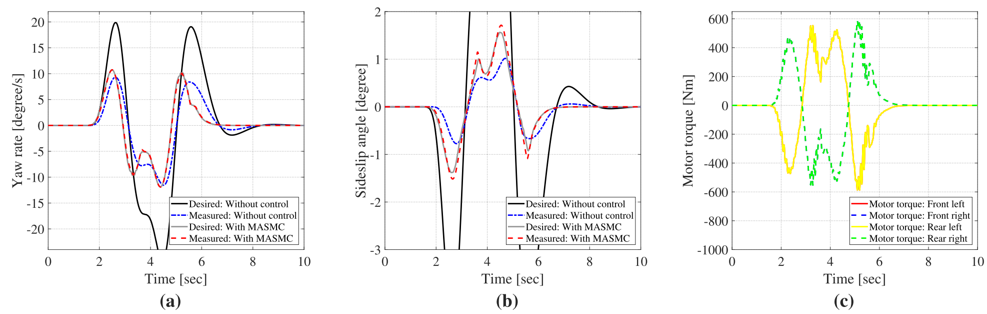

FIGURE 6. Driving data of MASMC without OTD. (a) Yaw rate. (b) Side-slip angle. (c) In-wheel-motor torque.

B. TORQUE DISTRIBUTION LAW

To solve the optimization problem, the least squares method is widely used. Based on equality constraints (34)–(36) and the concept of the friction circle, an optimization problem is formulated as follows:

$$\begin{aligned} &\text{minimize } J \\ &\text{subject to } Ax = y \end{aligned} \tag{40}$$

where

$$\begin{aligned} A &= \begin{bmatrix} \sin\delta_f & \cos\delta_f & \cos\delta_f & 1 & 1 \\ \cos\delta_f & \sin\delta_f & \sin\delta_f & 0 & 0 \\ l_f\cos\delta_f & l_f\sin\delta_f - \frac{d}{2}\cos\delta_f & l_f\sin\delta_f + \frac{d}{2}\cos\delta_f & -\frac{d}{2} & \frac{d}{2} \end{bmatrix} \\ x &= \begin{bmatrix} F^y_{f,d} & F^x_{fl,d} & F^x_{fr,d} & F^x_{rl,d} & F^x_{rr,d} \end{bmatrix}^\mathsf{T}, \quad y = \begin{bmatrix} F_{cmd} \\ ma_{y,d} - F^y_r \\ M_z + l_r F^y_r \end{bmatrix} \end{aligned} \tag{41}$$

The cost function J is defined as the sum of the squares of the individual wheel's workloads as follows:

$$J = \frac{1}{2}x^\mathsf{T}Qx = \frac{1}{2}\sum_{i=1}^{4}(\mu_{max}\eta_i) = \frac{1}{2}\sum_{i=1}^{4}\left(\frac{F_i^{x2}+F_i^{y2}}{F_i^{z2}}\right) \tag{42}$$

where

$$Q = \operatorname{diag}\left(\frac{2}{F_f^{z2}} + \frac{2(l_f/l_r)^2}{F_r^{z2}}, \frac{1}{F_{fl}^{z2}}, \frac{1}{F_{fr}^{z2}}, \frac{1}{F_{rl}^{z2}}, \frac{1}{F_{rr}^{z2}}\right) \tag{43}$$

Using Lagrange's theorem, the unique solution x_{opt} with respect to the optimization problem (40) is obtained as follows:

$$x_{opt} = Q^{-1}A^\mathsf{T}\left(AQ^{-1}A^\mathsf{T}\right)^{-1}y \tag{44}$$

The optimal torque command to the four-in-wheel-motors is calculated as follows:

$$T_{i,d} = rF^x_{i,d} \quad (i = fl, fr, rl, rr). \tag{45}$$

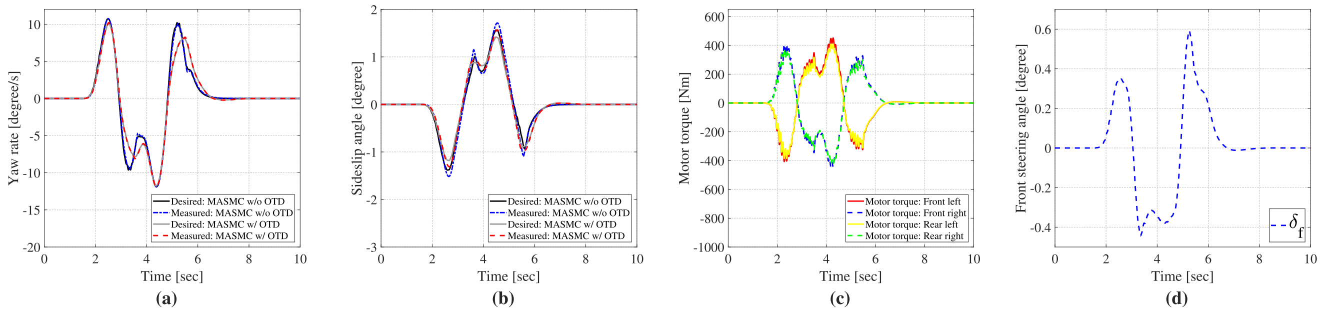

FIGURE 7. Driving data of MASMC without OTD. (a) Yaw rate. (b) Side-slip angle. (c) In-wheel-motor torque. (d) Front steering angle.

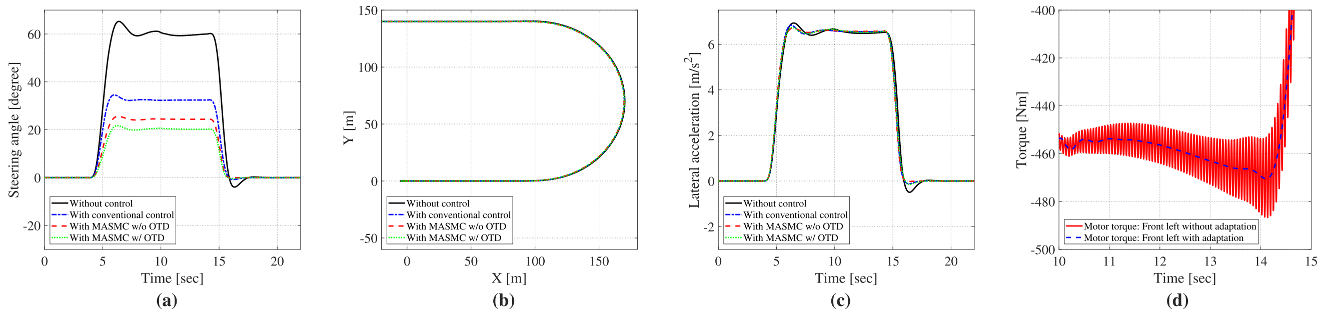

FIGURE 8. Comparsion of the three methods. (a) Steering wheel angle. (b) Trajectory. (c) Lateral acceleration. (d) Adaptation effect.

V. SIMULATION

A. SIMULATION SETUP

Two types of simulation scenarios were conducted to confirm the effectiveness of the proposed MASMC scheme. A simulation environment using the CarSim model and Matlab/Simulink was constructed for the implementation of the proposed MASMC scheme. The specifications for the simulation electric vehicle used in this study are presented in Table 1. The double-lane-change tests were carried out at $v_x = 100$ km/h on a high-μ road (i.e., $\mu = 1.0$) with path following mode. Otherwise, the cornering tests, which have a 70m radius, have been done on a high-μ road (i.e., $\mu = 1.0$) at $v_x = 77$ km/h with path following mode.

TABLE 1. Specifications of the simulation electric vehicle.

Total weight	2065 kg
Yaw moment of inertia	4973 kg$\cdot$m^2
Height of center of gravity (CoG)	0.56 m
Distance from CoG to front axle	1.48 m
Distance from CoG to rear axle	1.53 m
Track width	1.62 m
Effective wheel radius	0.327 m
Front cornering stiffness	111000 N/rad
Rear cornering stiffness	100000 N/rad
Max. Torque of IWM	600 N$\cdot$m

In the simulation, to better represent actual vehicle dynamics, we use Magic Formula-based tire model. The simulation results are obtained from four cases of control modes. The proposed MASMC is compared with results of without control, conventional lateral motion control method which is yaw tracking control with sliding mode control and the MASMC without optimal torque distribution [27], [28].

B. SIMULATION RESULTS

In the whole scenario, the driver attempts to follow the path by manipulating steering wheel in path following mode. Fig. 4–7 illustrate the first simulation scenario. These tests were performed to evaluate the transient-state performance of the proposed method. During the tests, according to (11), a reference yaw rate was created in conventional yaw rate tracking control. The two proposed methods are compared with the conventional method with identical control gains for fair comparison. Fig. 4 shows the comparison results of the three methods. The angle of the driver's steering wheel and manipulation effort, which must be reduced to improve handling performance, are shown in Fig. 4(a). We can confirm that the manipulation effort is reduced by the proposed MASMC. The adaptation effect, which decreased the burden of saturation function, is shown in Fig. 4(d). Fig. 5 represents the driving data of conventional yaw tracking control, which shows good yaw rate tracking performance. Fig. 6 represents the driving data of proposed MASMC without optimal torque distribution, showing the good side-slip angle tracking performance. Fig. 7 represents the driving data of the proposed MASMC compared to the driving data of the proposed MASMC without optimal torque distribution, seeing whether

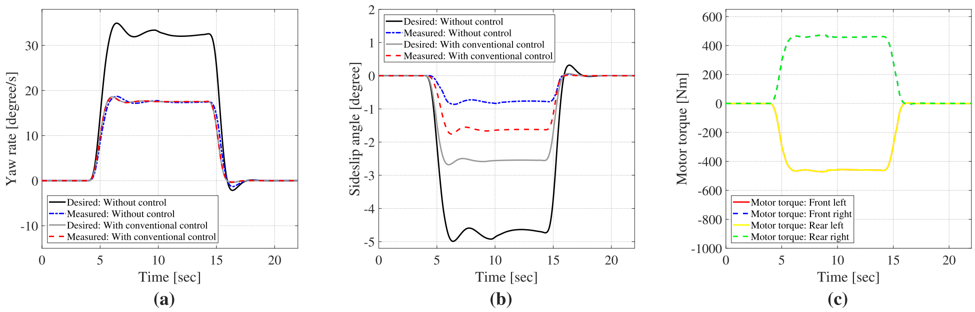

FIGURE 9. Driving data of conventional control. (a) Yaw rate. (b) Side-slip angle. (c) In-wheel-motor torque.

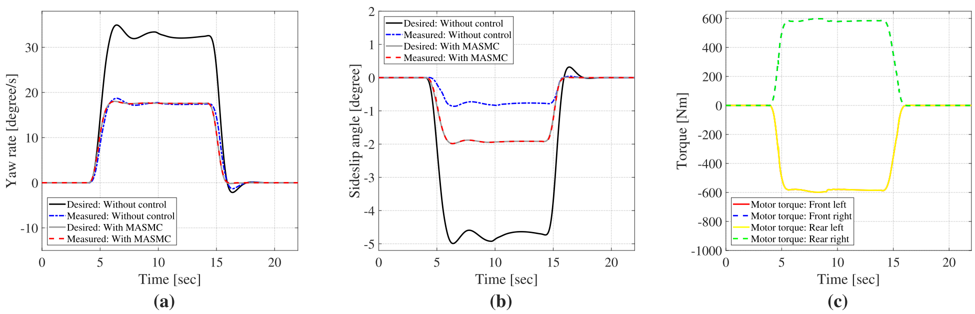

FIGURE 10. Driving data of MASMC without OTD. (a) Yaw rate. (b) Side-slip angle. (c) In-wheel-motor torque.

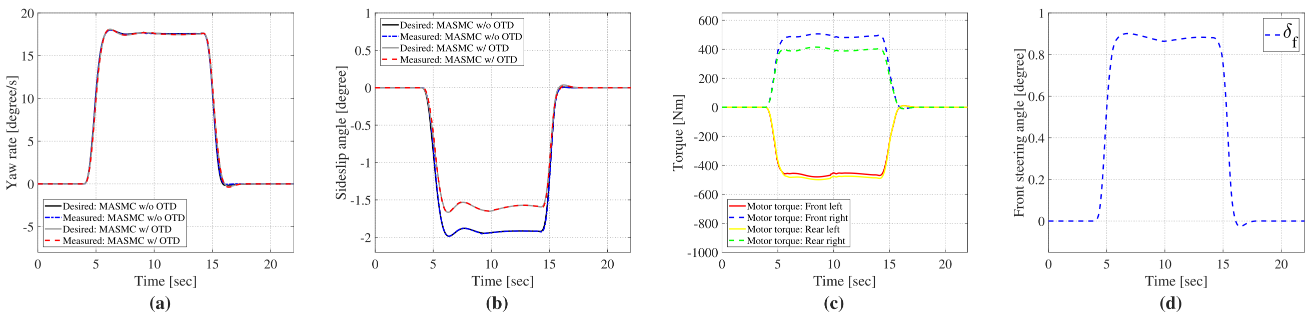

FIGURE 11. Driving data of MASMC with OTD. (a) Yaw rate. (b) Side-slip angle. (c) In-wheel-motor torque. (d) Front steering angle.

the three constraints in section IV are satisfied. Due to the optimal torque distribution law, the input of in-wheel-motor torque's redundancy is decreased.

Fig. 8–11 illustrate the second simulation scenario. These tests were performed to evaluate the steady-state performance of the proposed method. We can see that the steady-state manipulation effort, which is noticeably reduced by the proposed MASMC, is shown in Fig. 8(a). The adaptation effect, which decreased the burden of saturation function, is shown in Fig. 8(d). Fig. 9 represents the driving data of conventional yaw tracking control, which shows the good yaw rate tracking performance. Fig. 10 represents the driving data of the proposed MASMC without optimal torque distribution, showing the good side-slip angle tracking performance. Fig. 11 represents the driving data of the proposed MASMC compared to the driving data of the proposed MASMC without optimal torque distribution, seeing whether the three constraints in section IV are satisfied. Compared to the first simulation, the input of in-wheel motor torque redundancy is noticeably decreased by the optimal torque distribution law, which is composed of an active front steering system, as shown in Fig. 11(d).

VI. CONCLUSION

This paper has presented a new lateral motion control scheme based on the MASMC approach for improving the vehicle handling performance of an in-wheel-motor driven electric vehicle. The entire control system has a cascade-type control structure consisting of side-slip angle and yaw rate controllers. The cascade structure makes control system isolate a slow control loop in side-slip angle control. Furthermore, the parameter adaptation allows to reduce chattering while achieving the same tracking performance. To prove the stability of the entire system, Lyapunov stability theory is used. To solve the actuator redundancy problem, the optimal torque distribution solution based on the independent torque allocation is used. Simulation results based on the CarSim-MATLAB/Simulink platform verify the effectiveness of the proposed MASMC method. Compared to the conventional method, the proposed MASMC method can reduce manipulation effort (i.e., angle of driver's steering wheel), meaning improvement of the handling performance. This is one of the important results of this paper. It was shown that the torque distribution utilizing optimization contributes to balancing the control torque acting on each wheel. Through simulation results, it is confirmed that the vehicle motion control system based on the proposed MASMC method approach shows more dynamic characteristic (i.e., over steering characteristic) than the conventional method, and it can help driver realize the Fun to Drive keeping safety systems. Since the proposed control system is designed without considering actuator own efficiency, some energy loss may occur during control. Therefore, in future works, we will consider the efficiency of motor in optimal torque distribution law for enhancing aspect of efficiency.

APPENDIX

Nomenclature list:

$a_{y,d}$	Desired lateral acceleration at center of gravity (CG).
d	Track width.
h_{CG}	Vehicle height from center of gravity (CG).
l	Distance from front axle to rear axle.
l_f	Distance from CG to front axle.
l_r	Distance from CG to rear axle.
r	Wheel nominal radius.
v_x	Longitudinal velocity at CG.
v_y	Lateral velocity at CG.
m	Total mass of vehicle.
g	Acceleration due to gravity.
I_z	Yaw moment of inertia.
M_z	Yaw moment.
M_d	Yaw moment of disturbance.
C_f	Front tire cornering stiffness.
C_r	Rear tire cornering stiffness.
K_s	Vehicle stability factor.
i	1, 2, 3, and 4 corresponding to front left, front right, rear left, and rear right ($= fl, fr, rl, rr$).
F_i^x	Longitudinal tire force at the ith tire.
$F_{i,d}^x$	Longitudinal tire force, is created by optimal torque distribution, at the ith tire.
F_{fl}^x	Longitudinal force acting on the front left tire.
F_{fr}^x	Longitudinal force acting on the front right tire.
F_{rl}^x	Longitudinal force acting on the rear left tire.
F_{rr}^x	Longitudinal force acting on the rear right tire.
F_{cmd}	Longitudinal force command from acceleration pedal.
F_i^y	Lateral tire force at the ith tire.
F_f^y	Front lateral tire force ($= F_{fl}^y + F_{fr}^y$).
F_r^y	Rear lateral tire force ($= F_{rl}^y + F_{rr}^y$).
F_{fl}^y	Lateral force acting on the front left tire.
F_{fr}^y	Lateral force acting on the front right tire.
F_{rl}^y	Lateral force acting on the rear left tire.
F_{rr}^y	Lateral force acting on the rear right tire.
F_i^z	Vertical tire force at the ith tire.
F_{fl}^z	Vertical force acting on the front left tire.
F_{fr}^z	Vertical force acting on the front right tire.
F_{rl}^z	Vertical force acting on the rear left tire.
F_{rr}^z	Vertical force acting on the rear right tire.
$T_{i,d}^m$	In-wheel motor torque, is created by optimal torque distribution, applied to the ith tire.
T_{rl}^m	Rear left in-wheel motor torque.
T_{rr}^m	Rear right in-wheel motor torque.
α_f	Front tire slip angle.
α_r	Rear tire slip angle.
β	Vehicle side-slip angle.
β_d	Desired vehicle side-slip angle.
δ_f	Front steering angle.
γ	Yaw rate.
γ_d	Desired yaw rate.
μ	Road friction coefficient.
ω_i	Wheel angular velocity at the ith tire.
τ_γ	Relaxation time constant of desired yaw rate.
τ_β	Relaxation time constant of desired vehicle side-slip angle.

REFERENCES

[1] Y. Hori, "Future vehicle driven by electricity and control-research on four wheel motored 'UOT electric march II,'" *IEEE Trans. Ind. Electron.*, vol. 51, no. 5, pp. 954–962, Oct. 2004.

[2] S. Sakai, H. Sado, and Y. Hori, "Motion control in an electric vehicle with four independently driven in-wheel motors," *IEEE/ASME Trans. Mechatronics*, vol. 4, no. 1, pp. 9–16, Mar. 1999.

[3] D. Yin, S. Oh, and Y. Hori, "A novel traction control for EV based on maximum transmissible torque estimation," *IEEE Trans. Ind. Electron.*, vol. 56, no. 6, pp. 2086–2094, Jun. 2009.

[4] N. Mutoh and Y. Nakano, "Dynamics of front-and-rear-wheel-independent-drive-type electric vehicles at the time of failure," *IEEE Trans. Ind. Electron.*, vol. 20, no. 5, pp. 1488–1499, Mar. 2012.

[5] Y. Chen and J. Wang, "Fast and global optimal energy-efficient control allocation with applications to over-actuated electric ground vehicles," *IEEE Trans. Control Syst. Technol.*, vol. 20, no. 5, pp. 1202–1211, Sep. 2012.

[6] R. Wang and J. Wang, "Fault-tolerant control with active fault diagnosis for four-wheel independently driven electric ground vehicles," *IEEE Trans. Veh. Technol.*, vol. 60, no. 9, pp. 4276–4287, Nov. 2011.

[7] C. E. Beal and J. C. Gerdes, "Model predictive control for vehicle stabilization at the limits of handling," *IEEE Trans. Control Syst. Technol.*, vol. 21, no. 4, pp. 1258–1269, Jul. 2013.

[8] J. Zhu, K. W. E. Cheng, X. Xue, and Y. Zou, "Design of a new enhanced torque in-wheel switched reluctance motor with divided teeth for electric vehicles," *IEEE Trans. Magn.*, vol. 53, no. 11, Nov. 2017, Art. no. 2501504.

[9] G. De Filippis, B. Lenzo, A. Sorniotti, P. Gruber, and W. De Nijs, "Energy-efficient torque-vectoring control of electric vehicles with multiple drivetrains," *IEEE Trans. Veh. Technol.*, vol. 67, no. 6, pp. 4702–4715, Jun. 2018.

[10] M. Croft-White, "Measurement and analysis of rally car dynamics at high attitude angles," Ph.D. dissertation, Dept. Automot., Mech. Struct. Eng., Cranfield Univ., Cranfield, U.K., May 2006.

[11] N. Mutoh, T. Kazama, and K. Takita, "Driving characteristics of an electric vehicle system with independently driven front and rear wheels," *IEEE Trans. Ind. Electron.*, vol. 53, no. 3, pp. 803–813, Jun. 2006.

[12] K. Nam, S. Oh, H. Fujimoto, and Y. Hori, "Robust yaw stability control for electric vehicles based on active front steering control through a steer-by-wire system," *Int. J. Automot. Technol.*, vol. 13, no. 7, pp. 1169–1176, 2012.

[13] S. Inagaki, I. Kushiro, and M. Yamamoto, "Analysis on vehicle stability in critical cornering using phase-plane method," *JSAE Rev.*, vol. 16, no. 2, p. 216, 1995.
[14] H. Nozaki, "About the driver model and the improvement of vehicle movement performance at the drift cornering," (in Japanese), *Trans. JSME*, vol. 68, no. 675, pp. 3178–3185, 2006.
[15] M. Abdulrahim, "On the dynamics of automobile drifting," presented at the SAE Int., Detroit, MI, USA, 2006.
[16] J. Edelmann and M. Plöchl, "Handling characteristics and stability of the steady-state powerslide motion of an automobile," *Reg. Chaotic Dyn.*, vol. 14, no. 6, pp. 682–692, 2006.
[17] Q. Lu, P. Gentile, A. Tota, A. Sorniotti, P. Gruber, F. Costamagna, and J. De Smet, "Enhancing vehicle cornering limit through sideslip and yaw rate control," *Mech. Syst. Signal Process.*, vol. 75, pp. 455–472, Jun. 2016.
[18] K. Nam, H. Fujimoto, and Y. Hori, "Advanced motion control of electric vehicles based on robust lateral tire force control via active front steering," *IEEE/ASME Trans. Mechatronics*, vol. 19, no. 1, pp. 289–299, Feb. 2014.
[19] K. Nam, S. Oh, H. Fujimoto, and Y. Hori, "Estimation of sideslip and roll angles of electric vehicles using lateral tire force sensors through RLS and Kalman filter approaches," *IEEE Trans. Ind. Electron.*, vol. 60, no. 3, pp. 988–1000, Mar. 2013.
[20] W. Shen, Z. Pan, M. Li, and H. Peng, "A lateral control method for wheel-footed robot based on sliding mode control and steering prediction," *IEEE Access*, vol. 6, no. 3, pp. 58086–58095, 2018.
[21] N. Mutoh, T. Kazama, and K. Takita, "Driving characteristics of an electric vehicle system with independently driven front and rear wheels," *IEEE Trans. Ind. Electron.*, vol. 53, no. 3, pp. 803–813, Jun. 2006.
[22] M. Canale, L. Fagiano, A. Ferrara, and C. Vecchio, "Vehicle yaw control via second-order sliding-mode technique," *IEEE Trans. Ind. Electron.*, vol. 55, no. 11, pp. 3908–3916, Nov. 2008.
[23] L. De Novellis, A. Sorniotti, P. Gruber, and A. Pennycott, "Comparison of feedback control techniques for torque-vectoring control of fully electric vehicles," *IEEE Trans. Veh. Technol.*, vol. 63, no. 8, pp. 3612–3623, Oct. 2014.
[24] H. Fujimoto and S. Harada, "Model-based range extension control system for electric vehicles with front and rear driving–braking force distributions," *IEEE Trans. Ind. Electron.*, vol. 62, no. 5, pp. 3245–3254, May 2015.
[25] K. Maeda, H. Fujimoto, and Y. Hori, "Four-wheel driving-force distribution method for instantaneous or split slippery roads for electric vehicle," *Automatika*, vol. 54, no. 1, pp. 103–113, 2013.
[26] R. Wang, H. R. Karimi, N. Chen, G. Yin, and J. Wang, "Motion control of four-wheel independently actuated electric ground vehicles considering tire force saturations," *Math. Problems Eng.*, vol. 2013, Nov. 2013, Art. no. 819302.
[27] T. Goggia and A. Sorniotti, "Integral sliding mode for the torque-vectoring control of fully electric vehicles: Theoretical design and experimental assessment," *IEEE Trans. Veh. Technol.*, vol. 64, no. 5, pp. 1701–1715, May 2015.
[28] K. Nam, H. Fujimoto, and Y. Hori, "Design of an adaptive sliding mode controller for robust yaw stabilisation of in-wheel-motor-driven electric vehicles," *Int. J. Vehicle Des.*, vol. 67, no. 1, pp. 98–113, 2015.

MINSEONG CHAE received the B.S. degree in mechanical engineering from Yeungnam University, South Korea, in 2017. He is currently pursuing the master's degree. His research interests include advanced control systems and autonomous vehicles.

YOUNGJIN HYUN received the B.S. degree in mechanical engineering from Kyungpook National University, South Korea, in 1990, and the M.S. degree in mechanical engineering from Southampton University, U.K., in 2006. He finished the course works for Ph.D. Program in Seoul National University, South Korea, in 2018. He was a Chassis Engineer with Research and Development Division in Hyundai Motor Company, South Korea. He has enlarged research areas as a Visiting Scholar at the University of California, Berkeley, USA, in 2016, with Prof. Karl Hedrick. He had a lot of research experience for steering and suspension system and active control system of ground vehicles. His current research interests include advanced control systems and autonomous vehicles.

KYONGSU YI received the B.S. and M.S. degrees in mechanical engineering from Seoul National University, South Korea, in 1985 and 1987, respectively, and the Ph.D. degree in mechanical engineering from the University of California, Berkeley, in 1992. He is currently a Professor with the School of Mechanical and Aerospace Engineering, Seoul National University, South Korea. His research interests include control systems, driver assistant systems, and active safety systems of a ground vehicle. He currently serves as a member of the editorial boards of the KSME, IJAT, and ICROS journals.

KANGHYUN NAM (S'10–M'12) received the B.S. degree in mechanical engineering from Kyungpook National University, Daegu, South Korea, in 2007, the M.S. degree in mechanical engineering from the Korea Advanced Institute of Science and Technology, Daejeon, South Korea, in 2009, and the Ph.D. degree in electrical engineering from The University of Tokyo, Tokyo, Japan, in 2012.

From 2012 to 2015, he was a Senior Engineer with Samsung Electronics Company Ltd., Gyeonggi-do, South Korea. Since 2015, he has been an Assistant Professor with the School of Mechanical Engineering, Yeungnam University, Gyeongbuk, South Korea. His research interests include vehicle motion control, steer-by-wire system control, and in-wheel-motor-driven electric vehicles.

Prof. Nam is a member of the Korean Society of Automotive Engineers and an Associate Editor of the IEEE Transactions on Vehicular Technology. He received the Best Paper Award from the IEEE Transactions on Industrial Electronics, in 2014.